

Comparative studies of magnetic properties in osmates with the double perovskite structure

Cuihong Wang,¹ Yuanhui Xu,^{1,*} Weiyi Hao,² Runxue Wang,¹ Xipeng Zhang,¹ Keju Sun,¹ and Xianfeng Hao^{1,†}

¹Key Laboratory of Applied Chemistry, Yanshan University, Qinhuangdao 066004, People's Republic of China

²Tangshan No. 2 Middle School, Tangshan 063001, People's Republic of China

 (Received 12 October 2018; revised manuscript received 30 November 2018; published 14 January 2019)

Using the first-principles density functional approach, we comparatively studied the electronic and magnetic properties of two series of ordered double perovskite, Ba_2BOsO_6 ($B = Sc, Y, \text{ and } In$) and A_2ScOsO_6 ($A = Ba, Sr, \text{ and } Ca$). The electronic structure calculations indicate that the Os ion bears the nominal t_{2g}^3 state with oxidation state 5+ and is the only magnetically active one in all compounds. In nice agreement with the experimental observations, all of them stabilized in the type I antiferromagnetic alignment, which is mediated by the moderate nearest-neighbor antiferromagnetic interactions through the Os-O-B-Os 90° route and accompanied by mild next-nearest-neighbor antiferromagnetic coupling via the Os-O-B-Os 180° route, in spite of the geometric frustration. The mechanism of the antiferromagnetic interaction has been proposed based on the density of states analysis. In addition, the computed magnetic moment on Os ions, $\sim 2\mu_B$, is remarkably smaller than the ideal spin-only value. In conjunction with the modest spin-orbit coupling effect, strong covalency between the Os-5d and O-2p states reduces the magnetic moments. More importantly, our results demonstrated that the magnitude of the magnetic couplings as well as magnetic transition temperature T_N are directly proportional to the reciprocal of the absolute value of energy mismatch between the B -nd and occupied Os- t_{2g} band; in addition, they are also a function of the Sc-O-Os bond angles, i.e., the buckling of the octahedral connectivity. Moreover, comparison of these two series helps to identify the energy mismatch as the efficient factor to adjust the magnetic interactions.

DOI: [10.1103/PhysRevB.99.035126](https://doi.org/10.1103/PhysRevB.99.035126)

I. INTRODUCTION

Ordered double perovskite $A_2BB'O_6$, where the B and B' cations octahedrally coordinated by oxygen anions are arranged within a rocksalt pattern, have attracted a plethora of attention and are intensively studied over decades due to diverse interesting properties, such as high T_N ferrimagnetism (e.g., Ca_2FeOsO_6 [1] and Sr_2CrOsO_6 [2]), colossal magnetoresistance (e.g., Sr_2FeMoO_6 [3]), and Dirac-Mott insulator (e.g., Ba_2NiOsO_6 [4]). Apparently, the rich, strongly correlated electronic behaviors are intimately derived from the coupling between lattice, charge, orbital, and spin degrees of freedom of the different cations at B and B' sites. When both B and B' are magnetic ions, the magnetic and electronic properties are predominantly determined by the B -O- B' interactions, described as a double exchange or superexchange mechanism according to Goodenough's work [5]. However, if the B site ion is nonmagnetic, the magnetic properties are exclusively governed by the superexchange coupling through the B' -O- B -O- B' or B' -O-O- B' paths. Unlike the initial assumption that the nonmagnetic B cations are considered to play a negligible role in magnetic exchange interaction, nowadays, the effect of the electronic configurations of the nonmagnetic B cations have been highlighted [6–9]. The d -shell occupancy of nonmagnetic B cations strongly affects the hybridization between the B' - d and O-2p states and the

strength of exchange interaction, determining the magnetic ground state.

In recent times, the thrust in ordered double perovskite $A_2BB'O_6$ with nonmagnetic B cations has been concentrated on $4d/5d$ transition metal oxides, especially osmates. Various mixed nonmagnetic metal osmates with ideal cubic perovskite structure or a slight distortion have been reported and characterized. Examples include Sr_2BOsO_6 [10] ($B = Sc, Y, \text{ and } In, P2_1/n$), Ca_2BOsO_6 [11,12] ($B = Sc \text{ and } In, P2_1/n$), Ba_2BOsO_6 [13,14] ($B = Sc, Y, \text{ and } In, Fm-3m$), and La_2NaOsO_6 [15,16] ($P2_1/n$) with osmium taking the oxidation state Os (V) and t_{2g}^3 electronic configuration. Sr_2MgOsO_6 [17] ($I4/m$) embracing Os (VI) with $5d^2$ electronic configuration exhibits antiferromagnetic at 110 K, the highest temperature in this family. It is interesting to note that Ca_2MgOsO_6 [17] ($P2_1/n$) does not show any magnetic order even up to very low temperature. Besides, the cubic phase Ba_2NaOsO_6 [18,19] ($Fm-3m$) is a reported $5d^1$ ferromagnetic Mott insulator with formal valence of Os (VII) at $T_C = 6.8$ K.

Concerning the materials containing Os (V) with $5d^3$ electronic configuration, the majority [10–17] show a maximum at a temperature range of 14–93 K in temperature dependent magnetic susceptibilities, indicating the onset of long range antiferromagnetic ordering, which is attributed to the nearest-neighbor (NN) Os-O-B-Os superexchange interaction. Generally, the presence of NN antiferromagnetic coupling within the framework of edge-shared tetrahedra comprising the B' magnetic ions leads to magnetic frustration in systems. However, the type I antiferromagnetic

*yhxu@ysu.edu.cn

†xfhao@ysu.edu.cn

ordering on the B' sublattice is observed in neutron powder diffraction [20–22], in spite of the presence of frustration. Density functional calculations confirmed the assertion, and indicated the strong Os-O hybridization as well as spin-orbit coupling are responsible for the remarkable reduction of Os magnetic moments from the spin-only value of $\sim 3\mu_B$. The spin-orbit-induced anisotropy is considered to be essential for the realization of the antiferromagnetic ground state [22,23]. Furthermore, systematic theoretical studies on Sr_2BOsO_6 [7] ($B = \text{Sc}, \text{Y}, \text{and In}$) crystallized in monoclinic $P2_1/n$ structures through the first-principles calculations reveal the imperative role of open-shell (d^0) electronic configuration of the nonmagnetic cations in determining the magnetic exchange interactions, compared to the closed-shell (d^{10}) state. This discrimination seems to stem from different energy overlaps between Os-5d and B-d states, and justifies the experimentally observed substantial differences in magnetic transition temperatures [7]. Notice that Ba_2BOsO_6 [13,14] ($B = \text{Sc}, \text{Y}, \text{and In}$) stabilized in the ideal perovskite structure within the $Fm\bar{3}m$ space group, in which there is no structural distortion and the B-O-Os bond angles are 180° . Hence, this complex issue motivated us to explore the character of the nonmagnetic B cations in distortion-free analogs to establish the linkage between the magnetic exchange constants and the energy mismatch between Os-5d and B-d states. In addition, the buckling of the octahedral connections seems to exert an appreciable impact on the magnetic properties. It is essential to clarify the impact of the variation, i.e., the deviation of the B-O-Os bond angles from 180° , on the strength of the magnetic couplings. Uncovering the origin of the correlation is indispensable for the further in-depth understanding of the physics of ordered double perovskite containing nonmagnetic B and magnetic B' cations with $5d^3$ electronic configuration.

In this work, systematic investigations on electronic and magnetic properties of two series of ordered double perovskite $A_2\text{BOsO}_6$ with nonmagnetic B cations have been conducted via first-principles density functional theory (DFT). In addition, the spin-orbit coupling effect has been discussed. One is the Ba_2BOsO_6 ($B = \text{Sc}, \text{Y}, \text{and In}$) series with the ideal cubic $Fm\bar{3}m$ structure. The deduced magnetic coupling constants reveal that the NN interaction is substantially stronger than the next-nearest-neighbor (NNN) one, resulting in the type I magnetic ground state, in accordance with the experimental observations. Furthermore, the magnitude of the magnetic couplings as well as the magnetic transition temperature T_N are directly proportional to the reciprocal of the absolute value of energy mismatch between the B-nd and occupied Os- t_{2g} band. The smaller the energy mismatch, the larger the magnetic exchange coupling constants as well as the transition temperature. The other one is the $A_2\text{ScOsO}_6$ ($A = \text{Ba}, \text{Sr}, \text{and Ca}$) series with different degrees of buckling of octahedral connections from 180° to 151° . Our results indicate that the strengths of the magnetic interactions are related to the Sc-O-Os bond angles. The larger the structural distortion, the smaller the exchange coupling. Compared to the structural distortion, the energy mismatch is the principal factor to determine the magnetic coupling constants and, consequently, the critical transition temperature.

The cubic structure of Ba_2BOsO_6 ($B = \text{Sc}, \text{Y}, \text{and In}$) (Fig. 1, left) can be pictured as a framework consisting of alternative corners sharing untilted BO_6 and OsO_6 octahedra separated by Ba ions, which are located at the void positions among these two octahedra. Substitution of Ba cations in $\text{Ba}_2\text{ScOsO}_6$ with smaller isovalent cations, e.g., Sr and Ca, leads to the buckling of octahedral connectivity (Fig. 1, right), stabilized in the $P2_1/n$ phase. The deviation of the Sc-O-Os

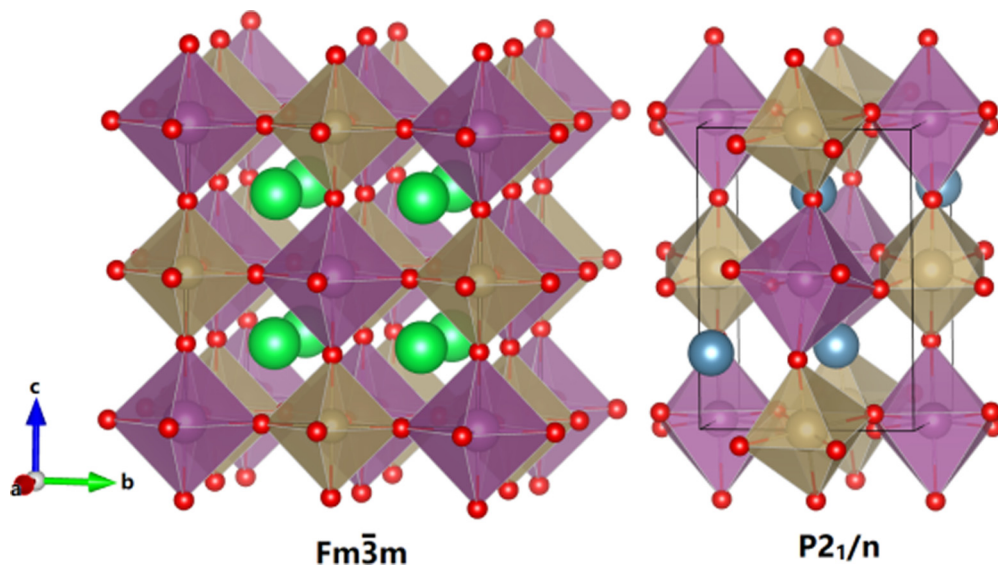


FIG. 1. (Left) Double perovskite structure of Ba_2BOsO_6 ($B = \text{Sc}, \text{Y}, \text{and In}$) within the $Fm\bar{3}m$ space group, in which the Os atoms (medium purple spheres) and the B atoms (medium brown ones) are surrounded by the O_6 octahedron denoted by small red spheres, while the big green spheres are Ba atoms. (Right) Double perovskite structure of $A_2\text{ScOsO}_6$ ($A = \text{Sr}$ and Ca) within the $P2_1/n$ space group. The medium brown and purple spheres are Sc and Os atoms, respectively. Small red spheres are oxygen atoms, the big blue ones are the A ($A = \text{Sr}$ and Ca) atoms. Rotation and tilting of the O_6 octahedra lead into the bend of the Sc-O-Os angle from 180° in the cubic phase to an average value of 166° in $\text{Sr}_2\text{ScOsO}_6$ and 151° in $\text{Ca}_2\text{ScOsO}_6$.

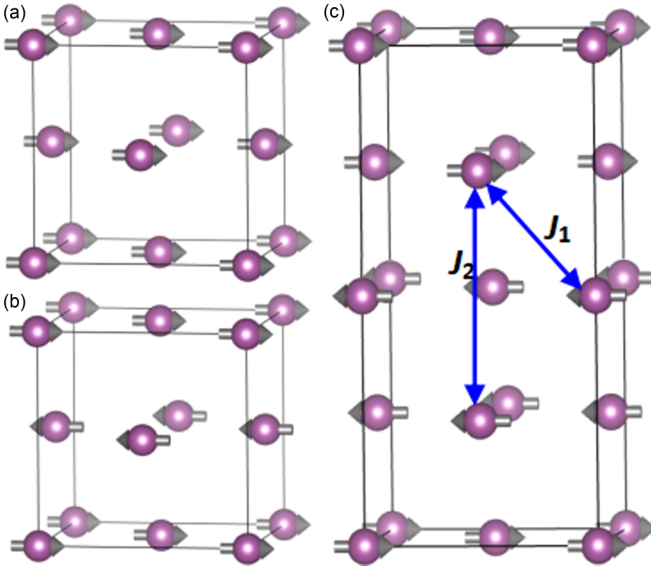


FIG. 2. Three magnetic ordering configurations [ferromagnetic (FM) (a), antiferromagnetic type I (AFM-I) (b), and antiferromagnetic type II (AFM-II) (c)] considered for double perovskite osmates. The arrows indicate magnetic moment orientation on Os atoms. The blue arrows labeled as J_1 and J_2 are the exchange pathways between Os^{5+} ions in the sublattice, where the J_1 are the nearest-neighbor exchange coupling constants through the Os-O-B-O-Os (90°) paths, while the J_2 are the next nearest-neighbor exchange coupling constants via the Os-O-B-O-Os (180°) paths. Notice that, although the rotation and tilting of the O_6 octahedra are present in the monoclinic $P2_1/n$ phase ($\text{Sr}_2\text{ScOsO}_6$ and $\text{Ca}_2\text{ScOsO}_6$), the anisotropy of the exchange paths are neglected for simplicity.

bond angles from the ideal one (180°) is dependent on the radii of substitutable ions, 165° for Sr and 151° for Ca [10].

Notice that the theoretical optimized lattice parameters and atomic positions of all atoms are in good agreement with the experimental values with deviations smaller than 1.4%. The errors introduced by the volume disparity are unlikely to have a significant impact on the tendency along the series. Therefore, our studies were accomplished based on the experimental crystal structures. The spin-polarized DFT calculations are achieved with the plane-wave basis set

as implemented in the Vienna *ab initio* simulation package [24,25]. The generalized gradient approximation (GGA) exchange correlation functional is adopted according to the Perdew-Burke-Ernzerhof scheme [26] to investigate the electronic properties. In order to explore electron correlation of the Os-5d shell, the additional DFT + U calculations [27,28] with double counting corrections were performed. Values of the screened Coulomb interaction U were tested by changing from 0.0 to 2.0 eV, in line with values reported for 5d oxides [7,29]. For electronic structure calculations, a plane-wave energy cutoff of 500 eV was employed. The k -point meshes over the total Brillouin zone were sampled by $4 \times 4 \times 4$ and $6 \times 6 \times 4$ grids constructed according to the Monkhorst-Pack scheme [30,31] for cubic and monoclinic phases, respectively. Moreover, we carried out the noncollinear magnetic calculations with fully unconstrained formalism [32] to explicitly include the spin-orbit coupling (SOC) [33] effect.

II. Ba_2BOsO_6 ($B = \text{Sc}, \text{Y}, \text{and In}$) series

We performed electronic calculations on three distinct magnetic alignments: ferromagnetic (FM) and two distinct antiferromagnetics (AFM) as shown schematically in Fig. 2, within the normal GGA + U ($U_{\text{eff}} = 0.0, 1.0, \text{ and } 2.0$ eV) prescription with the goal of determining the nature of the magnetic ground state. The AFM-I case is the type I antiferromagnetic pattern resolved from neutron diffraction analysis [20–22], where the in-plane NN relative orientations are FM, while out-of-plane NN couplings are completely AFM and the NNN exchange interactions are FM. In the AFM-II pattern, in-plane NN coupling is FM; four of eight out-of-plane interactions are FM, while the others are AFM; and the NNN interactions are also AFM. Our results are summarized in Table I. We found the AFM-I type is the ground state, irrespective of the Hubbard U values, affirming the experimental observations [20]. Moreover, the GGA + U schemes prefer very stable magnetic solutions for each spin ordering with almost identical values of the magnetic moment of Os ($\sim 2 \mu_B$), which increase as a function of the Hubbard U values. The moment at the Os site reduces appreciably, and the surrounding oxygen atoms acquire substantial moment ($\sim 0.1 \mu_B$) due to the strong hybridization.

TABLE I. Computed total energies of two antiferromagnetic configurations with respect to the ferromagnetic one (per formula unit) and the deduced exchange interactions constants J_1 , J_2 as well as the theoretical Néel temperatures for Ba_2BOsO_6 ($B = \text{Sc}, \text{Y}, \text{ and In}$) and A_2ScOsO_6 ($A = \text{Ba}, \text{Sr}, \text{ and Ca}$) series acquired from the GGA/GGA + U ($U_{\text{eff}} = 1.0$ and 2.0 eV) methods. The experimental Néel temperatures taken from the literature are listed for comparison.

	$\text{Ba}_2\text{InOsO}_6$			Ba_2YOsO_6			$\text{Ba}_2\text{ScOsO}_6$			$\text{Sr}_2\text{ScOsO}_6$			$\text{Ca}_2\text{ScOsO}_6$		
	U_0	U_1	U_2	U_0	U_1	U_2	U_0	U_1	U_2	U_0	U_1	U_2	U_0	U_1	U_2
FM (meV)	0.00	0.00	0.00	0.00	0.00	0.00	0.00	0.00	0.00	0.00	0.00	0.00	0.00	0.00	0.00
AFM-I (meV)	-58.6	-44.5	-35.3	-124.2	-93.3	-71.1	-140.3	-121.0	-92.5	-137.4	-108.7	-86.1	-104.4	-77.9	-59.2
AFM-II (meV)	-33.2	-24.0	-18.7	-72.9	-52.1	-39.0	-78.3	-69.2	-50.6	-78.9	-60.5	-46.4	-61.7	-43.7	-31.8
J_1 (meV)	-1.63	-1.24	-0.98	-3.45	-2.59	-1.98	-3.90	-3.36	-2.57	-3.82	-3.02	-2.39	-2.90	-2.16	-1.64
J_2 (meV)	-0.32	-0.20	-0.12	-1.20	-0.61	-0.38	-0.91	-0.96	-0.49	-1.13	-0.68	-0.37	-1.05	-0.53	-0.24
T_N (K)	132.3	109.5	91.9	191.7	194.8	162.3	294.2	222.3	213.1	245.7	231.5	212.8	152.8	159.3	148.6
T_N (K) expt.		28			67.69			93			92			69	

Next we have deduced the exchange interactions to provide further insight into the magnetic properties and geometrical frustration for these osmates, based on the Heisenberg spin Hamiltonian [34]: $H = -\sum_{i,j} J_{i,j} \cdot S_i S_j$ where $J_{i,j}$ is an exchange interaction between the spins located at site i and j , $J > 0 (< 0)$ is ferromagnetic (antiferromagnetic) interactions, and $S = 3/2$ is the spin-only of $\text{Os}^{5+}5d^3$ ions. Here, we just focus on the first two nearest-neighbor exchange coupling interactions, NN J_1 versus NNN J_2 illustrated in Fig. 2 as arrows, and omitted the remote ones owing to the large distances. The computed exchange parameters are also listed in Table I. It is worth noting that the inclusion of the Hubbard U corrections give the same qualitative trend of exchange coupling constants for the Ba_2BOsO_6 ($B = \text{Sc}, \text{Y},$ and In) series, except for a slight decrease in absolute value.

Two intriguing aspects can be identified from the numbers. On one hand, the NN J_1 exchange coupling is almost four times bigger than the NNN J_2 one for all three compounds. The stronger exchange interactions can be traced back to the relatively shorter Os-Os distances linked by a 90° ligand network for the nearest-neighbor positions. Interestingly, both of the two magnetic interactions are AFM in nature. The combination of NN antiferromagnetic interactions within the edge-shared tetrahedra in the fcc arrangement of magnetic ions gives rise to magnetic frustration. Together with the AFM interactions between the Os atoms, the magnetic frustrated feature is in nice accordance with the aforementioned experimental observations [20–22]. On the other hand, the magnitude of relevant exchange interactions is largest in $\text{Ba}_2\text{ScOsO}_6$, smallest in $\text{Ba}_2\text{InOsO}_6$. To be specific, the NN coupling constants of $\text{Ba}_2\text{ScOsO}_6$ are almost three times larger than that of $\text{Ba}_2\text{InOsO}_6$, while the NNN interactions are roughly four times stronger than for $\text{Ba}_2\text{InOsO}_6$. Nonetheless, the corresponding exchange couplings in Ba_2YOsO_6 are somewhat weaker than that of $\text{Ba}_2\text{ScOsO}_6$. Given the exactly identical crystal structure, the tiny difference in crystal volumes could not account for the remarkable variation of the exchange constants. Summing up, these facts indicate that the diamagnetic B cations play a vital role in determining the magnetic interactions. Presumably, this interesting scenario is originated from the different energy mismatch between the B - nd and Os- $5d$ band as discussed in the following.

To trace the mechanisms behind individual magnitudes of magnetic interactions in these three osmates, it is informative to put the atomic projected density of states for the AFM-I ground state together for comparison as shown in Figs. 3(a)–3(c). The contribution of the Ba state to the valence and conduction band is negligibly small, indicating a high degree of ionic bonding between Ba and the host lattice, and is not shown in the figure for simplicity. In addition, the empirical Hubbard U value merely drives the insulating solution with different finite band gap, while the physics behind it remains unchanged.

The common characteristic feature of electronic structure for these three osmates is that the occupied Os- t_{2g} states are separated from the completely empty e_g states by an energy interval of ~ 4 eV, accompanied by a moderate spin splitting of ~ 2 eV. As a consequence, electronic configuration is close to the nominal t_{2g}^3 state and the oxidation state is $5+$. The Os- t_{2g} states around the Fermi level are strongly admixed

with O- $2p$ states. Besides, there are some Os- e_g orbitals present around -5 eV below the Fermi level merged with the O- $2p$ manifold, unfolding the strong covalency between the Os- $5d$ and O- $2p$ states. The covalent bonding is so strong that the computed Os magnetic moment ($\sim 2 \mu_B$) is remarkably smaller than the ideal spin-only value ($\sim 3 \mu_B$). This scenario is compatible with the experimentally measured effective magnetic moments [14]. In addition, a small but finite magnetic moment ($\sim 0.1 \mu_B$) appears at the surrounding O sites. In contrast to the Os- $5d$ and O- $2p$ states, the B - d ($B = \text{Sc}, \text{Y},$ and In) states make a negligible contribution towards the electronic properties around the Fermi level. All the B cations are nonmagnetic with zero magnetic moment.

The major electronic difference of the plots is the positions of the B - d states. For $\text{Ba}_2\text{ScOsO}_6$, the Sc- $3d$ states are fully empty and located 3.5 eV above the Fermi level, while the Y- $4d$ states are located at 4.5 eV above the Fermi level, suggesting Sc/Y cations possess a $3+$ oxidation state with d^0 electronic configuration. The extent of Y- $4d$ states is substantially wider than that of Sc- $3d$ states. Instead, the In- $4d$ states in $\text{Ba}_2\text{InOsO}_6$ are entirely occupied, centered around -14.0 eV below the Fermi level, confirming the closed shell of In^{3+} ($4d^{10}$ electronic configuration). The specific locations of the individual B - d states are important, since the principal superexchange couplings involve the B ions via Os-O- B -O-Os pathways, both the NN 90° and NNN 180° case.

We recall the difference of magnetic coupling constants in these three compounds as discussed above. Experimentally, the Néel temperature for $\text{Ba}_2\text{ScOsO}_6$ is 93 K, for Ba_2YOsO_6 is 69 K, and for $\text{Ba}_2\text{InOsO}_6$ is 28 K [14]. How these subtle electronic properties affect the magnetism and how they can explain the observed different T_N should be explored further. For these purposes, we illustrated the exchange constants, J_1 and J_2 , as a function of the reciprocal of the absolute value of the energy difference between B - nd and the occupied Os- t_{2g} band ($|\Delta\varepsilon|$) in Fig. 3(d). Undoubtedly, the progressive decrease of the energy difference leads to the monotonous increase of the magnitude of exchange coupling on the basis of the virtual hopping model as discussed later. Furthermore, we have evaluated the Néel transition temperature within the molecular field theory [35] from the knowledge of J_1 and J_2 . As expected, the theoretical transition temperature is directly proportional to the reciprocal of the absolute value of the energy difference between the B - nd and filled Os- t_{2g} band, as demonstrated in Fig. 3(e) along with the experimental values. The variation tendency of the computed T_N is in perfect accordance with the experimental results [10,14]. It is worth noting that the errors produced by the small volume differences are unlikely to change this trend. This fact indicates that our theoretical results are straight and trustworthy and the GGA + U method employed is reliable. Therefore, we explicitly arrived at the conclusion that the energy difference between the B - nd and occupied Os- t_{2g} band is a crucial quantity to explain the evolution of the superexchange interactions and the magnetic ordering temperature. The smaller the energy mismatch, the larger the magnetic exchange coupling constants and the transition temperature.

The mechanism of superexchange interaction in Ba_2BOsO_6 ($B = \text{Sc}, \text{Y},$ and In) is elucidated schematically in Fig. 3(f) where the positions of the atomic levels

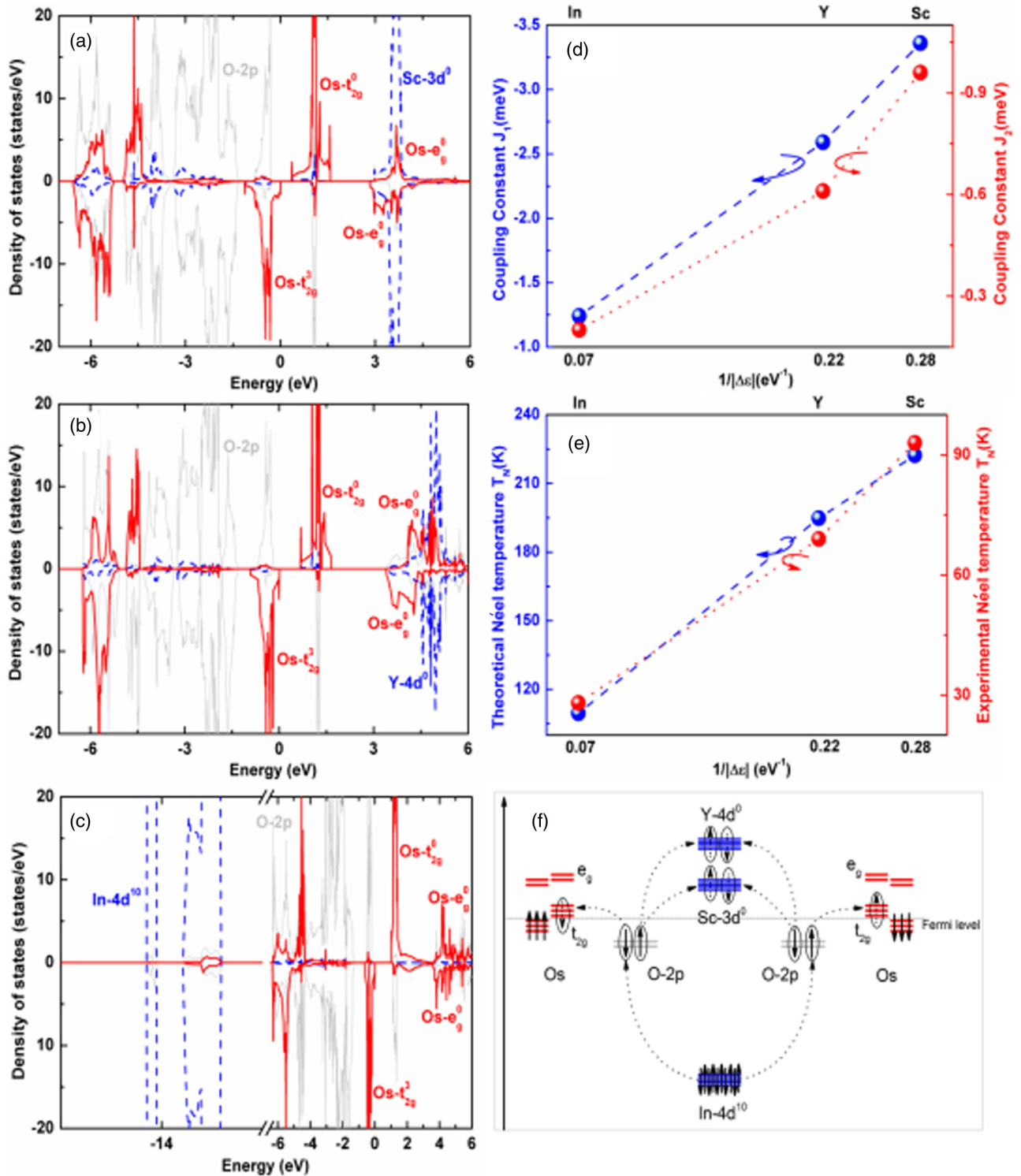


FIG. 3. Density of states projected on the Sc-3d (a), Y-4d (b), and In-4d (c) states, along with the Os-5d and O-2p states for Ba_2BOsO_6 ($B = \text{Sc}, \text{Y},$ and In) within the AFM-I configuration, obtained from the GGA + U ($U_{\text{eff}} = 1.0$ eV) calculations. Majority and minority spin are presented in the top and bottom channels, respectively. The Fermi level is set at zero on the energy scale. (d,e), Dependency of the relevant magnetic quantities [J_1 , J_2 , and T_N obtained with the GGA + U ($U_{\text{eff}} = 1.0$ eV) scheme] on the reciprocal of the energy mismatch between the B - nd and Os-5d band in the Ba_2BOsO_6 ($B = \text{Sc}, \text{Y},$ and In) series. For comparison, the experimental T_N values are included. Apparently, the amplitude of the magnetic interaction is inversely proportional to the energy mismatch between the B - nd and Os-5d band. (f) Schematic representation of the superexchange interaction through the Os-O-B-O-Os paths, which are derived from the partial density of states plots. The virtual electron hopping between Os- e_g , O-2p, and Sc-3d⁰, Y-4d⁰ as well as In-4d¹⁰ results in the antiferromagnetic coupling among Os⁵⁺ ions.

TABLE II. Calculated spin, orbital, and total ($m_{\text{tot}} = m_s + m_l$) moments (μ_B) of Os ions, the spin moments (μ_B) of O ions, the band gap (eV), and magnetocrystalline anisotropy energy (meV) presented in four spin directions ([001], [100], [110], and [111]) for Ba_2BOsO_6 ($B = \text{Sc, Y, and In}$) and A_2ScOsO_6 ($A = \text{Ba, Sr, and Ca}$) series obtained from the GGA + U ($U_{\text{eff}} = 1.0$ eV) scheme.

	m_s (Os) (μ_B)	m_l (Os) (μ_B)	m_{tot} (Os) (μ_B)	m (O) (μ_B)	ΔE (meV)	gap (eV)
Ba₂InOsO₆						
GGA+SOC+ U (100)	1.87	-0.13	1.74	0.10	0.0	0.67
GGA+SOC+ U (001)	1.87	-0.14	1.73	0.10	-2.2	0.92
GGA+SOC+ U (110)	1.86	-0.14	1.72	0.10	-0.3	0.84
GGA+SOC+ U (111)	1.85	-0.14	1.71	0.10	-0.9	0.86
GGA + U	2.01		2.01	0.10		0.99
Ba₂YO₆						
GGA+SOC+ U (100)	1.97	-0.08	1.89	0.08	0.0	0.57
GGA+SOC+ U (001)	1.96	-0.08	1.87	0.09	-3.5	0.67
GGA+SOC+ U (110)	1.98	-0.08	1.90	0.09	0.0	0.57
GGA+SOC+ U (111)	1.96	-0.09	1.87	0.09	-1.2	0.61
GGA + U	2.09		2.09	0.09		0.67
Ba₂ScOsO₆						
GGA+SOC+ U (100)	1.87	-0.08	1.80	0.09	0.0	0.38
GGA+SOC+ U (001)	1.86	-0.09	1.77	0.09	-5.2	0.35
GGA+SOC+ U (110)	1.84	-0.09	1.75	0.09	-0.2	0.28
GGA+SOC+ U (111)	1.86	-0.08	1.77	0.09	-2.5	0.31
GGA + U	2.01		2.01	0.11		0.35
Sr₂ScOsO₆						
GGA+SOC+ U (100)	1.82	-0.10	1.73	0.09	0.0	0.23
GGA+SOC+ U (001)	1.81	-0.10	1.71	0.09	-6.0	0.28
GGA+SOC+ U (110)	1.82	-0.09	1.73	0.09	-0.5	0.22
GGA+SOC+ U (111)	1.82	-0.10	1.72	0.09	-2.5	0.22
GGA + U	1.96		1.96	0.09		0.32
Ca₂ScOsO₆						
GGA+SOC+ U (100)	1.95	-0.09	1.87	0.10	0.0	0.61
GGA+SOC+ U (001)	1.94	-0.09	1.85	0.10	-2.0	0.68
GGA+SOC+ U (110)	1.97	-0.08	1.89	0.10	1.5	0.58
GGA+SOC+ U (111)	1.97	-0.09	1.88	0.10	-2.5	0.64
GGA + U	2.09		2.09	0.10		0.73

approximately correspond to their locations in the density of states plots. Provided that the electronic configuration of Os^{5+} is $t_{2g}^{3\uparrow}$, the O- $2p^\downarrow$ electron has a higher hopping amplitude to the $\text{Os}^{5+}-t_{2g}^\downarrow$ states than the O- $2p^\uparrow$ electron because the crystal field splitting between the t_{2g} and e_g states is larger than the spin splitting. Due to the nonmagnetic nature of the B cations, the virtual O- $2p$ electrons hopping towards Sc/Y- d^0 states prefer an antiparallel pattern, while the virtual In- $4d$ electrons hopping to $2p$ states of bilateral O anions maintain antiparallel alignment, leading into the antiferromagnetic coupling between $\text{Os}^{5+}-\text{Os}^{5+}$ pairs through the Os-O- B -O-Os paths, regardless of NN 90° or NNN 180° routes. This explains why Ba_2BOsO_6 ($B = \text{Sc, Y, and In}$) are antiferromagnetic. The hopping amplitude is inversely proportional to the absolute value of the difference between the B - nd and occupied Os- t_{2g} band in energy ($|\Delta\varepsilon|$) [5,36]. The larger the energy mismatch, the smaller the hopping amplitude; as a result, the smaller are the magnetic interaction constants as well as the Néel temperature.

To examine the effect of the spin quantization direction on electronic structure, we carried out the addition GGA + U + SOC calculations for the AFM-I ground state. The spin,

orbital, and total moments computed using the GGA + U + SOC method with $U_{\text{eff}} = 1.0$ eV are summarized in Table II, together with the band gap. A finite but small orbital moment ($\sim -0.1 \mu_B$) at the Os site appears with its direction opposite to the spin moment, irrespective of the spin quantizations considered. This situation is in good agreement with the previous reports [37,38], while it is in contrast with the assumption that the d^3 systems generally possess spin-only $S = 3/2$ ground states with quenched orbital angular momentum on the basis of the L-S coupling scheme. Apparently, the presence of SOC further reduces the total magnetic moment at the Os site, in addition to the covalency effect. The introduction of the SOC effect impelled the shrinking of the band gap, compared to the regular GGA + U calculations. The moderate SOC effect in $5d^3$ systems, however, does not surmount the crystal field, electron correlation effect, rendering the mechanism of antiferromagnetic coupling proposed above still valid.

III. A_2ScOsO_6 ($A = \text{Ba, Sr, and Ca}$) series

In $\text{Ba}_2\text{ScOsO}_6$, when Ba^{2+} is replaced by smaller cations Sr^{2+} or Ca^{2+} , the octahedral rotation emerges to optimize the

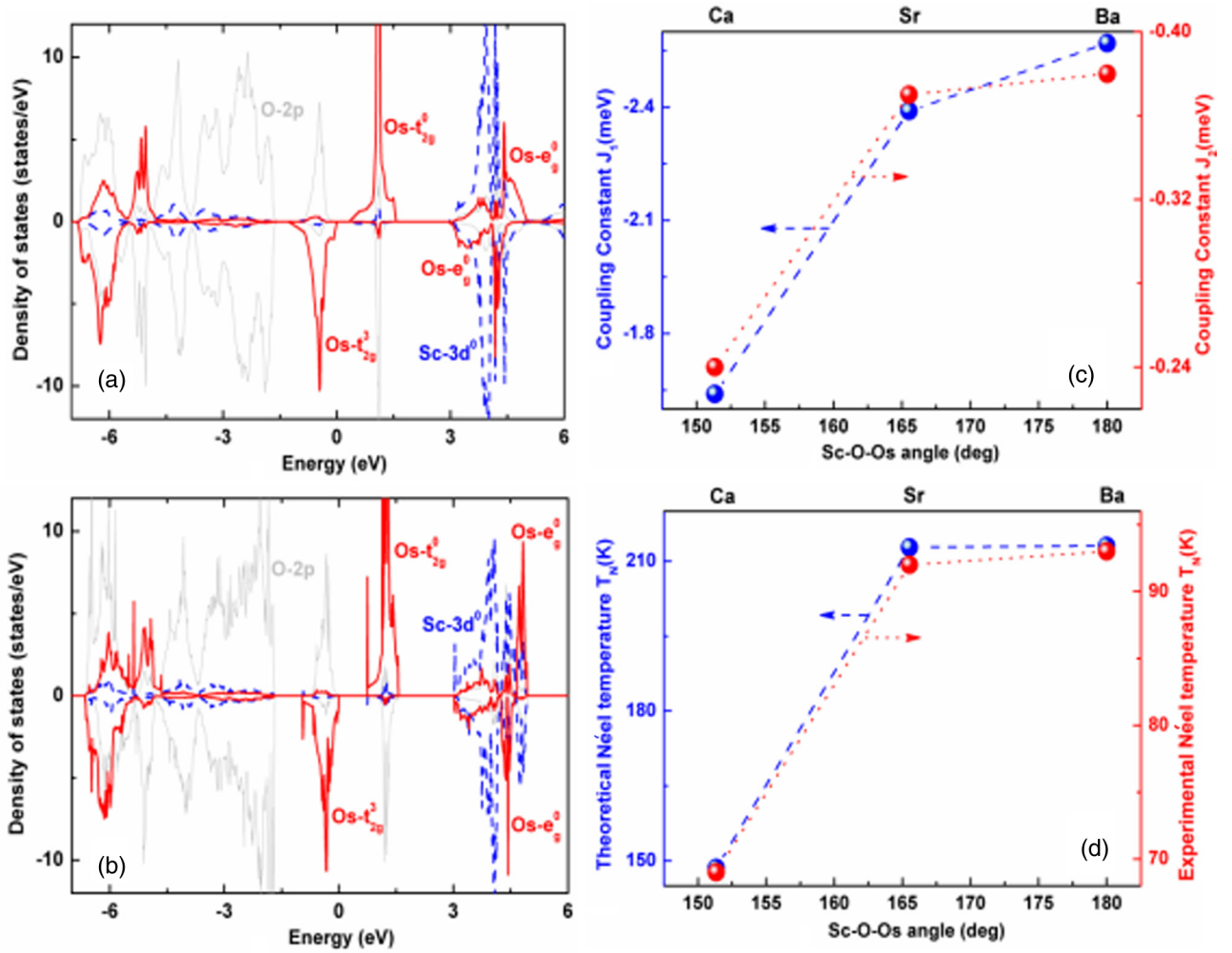


FIG. 4. Density of states projected on the Sc-3d, Os-5d, and O-2p states for $A_2\text{ScOsO}_6$ [$A = \text{Sr}$ (a), Ca(b)] within the AFM-I configuration, ground magnetic state, obtained from the GGA + U ($U_{\text{eff}} = 1.0$ eV) calculations. Majority and minority spin are presented in the top and bottom channels, respectively. The Fermi level is set at zero on the energy scale. (c,d) Dependency of the relevant magnetic quantities [J_1 , J_2 , and T_N achieved at the GGA + U ($U_{\text{eff}} = 2.0$ eV) level] on the the Sc-O-Os angle in the $A_2\text{ScOsO}_6$ ($A = \text{Ba}$, Sr, and Ca) series. For comparison, the experimental T_N values are included.

coordination environment of the smaller cations, distorting the crystal structure. In $\text{Sr}(\text{Ca})_2\text{ScOsO}_6$, it results in the $P2_1/n$ space group, squashing the Sc-O-Os bond angles to $165^\circ(151^\circ)$ [9] from the ideal one of 180° . Presumably, the shrinking of the bond angles leads to the progressive attenuation of Os- t_{2g} /O-2p hybridization and the reduction of the magnetic interactions and, consequently, the critical transition temperatures [5,39]. Actually, the experimental Néel temperature is 92 K for $\text{Sr}_2\text{ScOsO}_6$ and 69 K for $\text{Ca}_2\text{ScOsO}_6$ [10,14], which are slightly smaller than that of $\text{Ba}_2\text{ScOsO}_6$ 93 K [14].

In order to shed light on the effect of the buckling of octahedral connections, we examined the relation between exchange coupling and structural variations, electronic as well as magnetic properties. Following the same procedure in the Ba_2BOsO_6 ($B = \text{Sc}$, Y, and In) series, we firstly ascertained the magnetic ground state for $\text{Sr}_2\text{ScOsO}_6$ and $\text{Ca}_2\text{ScOsO}_6$. Identical with $\text{Ba}_2\text{ScOsO}_6$, the type I antiferromagnetic pattern is confirmed as the ground state (Table I) for both compounds, in nice agreement with the experimental determination on $\text{Sr}_2\text{ScOsO}_6$ [21,22] and previous theoretical

result [7]. Next, the symmetric magnetic exchange couplings have been estimated by mapping the DFT total energies onto the corresponding Ising model [34]. Notice that the splittings of monoclinic distortion have been ignored for the NN J_1 and NNN J_2 , in order to straightforwardly compare to the $\text{Ba}_2\text{ScOsO}_6$ case. That is, the J_1 (J_2) is the average NN (NNN) exchange coupling in this situation. Similar to $\text{Ba}_2\text{ScOsO}_6$, the NN J_1 exchange coupling is roughly four times larger than the NNN J_2 one. Both are negative, antiferromagnetic in nature. The antiferromagnetic character can be understood in the framework of superexchange interactions through the virtual hopping bridged by the d^0 open shell or d^{10} closed shell, demonstrated in Fig. 3(f). The addition of the Hubbard U penalty leads to a slight decrease in the absolute values of exchange coupling constants.

More importantly, we have found that the NN J_1 as well as NNN J_2 diminish mildly as a function of the Sc-O-Os bond angle from 180° (Ba) to 151° (Ca) in the $A_2\text{ScOsO}_6$ ($A = \text{Ba}$, Sr, and Ca) series as represented in Fig. 4(c). The decrease in J_1 and J_2 values can be attributed to the

reduction of hybridization between the filled Os- t_{2g} and O-2*p* orbitals, in particular for the topmost valence states spreading from -1.5 eV to the Fermi level. This is evidenced from the density of states plots of Sr₂ScOsO₆ and Ca₂ScOsO₆ shown in Figs. 4(a) and 4(b), compared to that of Ba₂ScOsO₆. The decreasing bandwidth of hybridized bands observed when going from Ba (1.1 eV) to Ca (1.0 eV) is in relation to the buckling of octahedral connections from 180° (Ba) to 151° (Ca). Moreover, the corresponding theoretical Néel temperatures validated this assertion, as depicted in Fig. 4(d). The trend of computed T_N is consistent with experimental observations [10,14], corroborating the approximation of neglecting the splitting effect of monoclinic distortion. What we found so far is enough to strongly suggest that the buckling of octahedral connections will decrease hybridization between the Os- t_{2g} and O-2*p* orbitals when going from Ba to Ca, which diminishes the magnitude of the overall magnetic exchange couplings and decreases the Néel temperatures of this series.

As stated above, although the L-S coupling description is not sufficient for Os⁵⁺-5*d*³ electronic configuration, the modest spin-orbit coupling effect, as manifested from the computed orbital moment on Os sites (listed in Table II), is not strong enough to destroy the main character of the electronic structure underlying the antiferromagnetic interactions.

IV. DISCUSSION

The computational investigations of this study allow us to clarify the electronic and magnetic properties of two series of ordered double perovskite A_2BOsO_6 with nonmagnetic B^{3+} cations. The electronic structure results show that the Os ion bears the nominal t_{2g}^3 state with oxidation state 5+ and is the only magnetically active one in all compounds we studied. Notwithstanding the magnetic frustration, all of them stabilized in type I antiferromagnetic alignment, which is mediated by the moderate NN antiferromagnetic interactions through the Os-O-B-O-Os 90° route, assisted with the mild NNN antiferromagnetic coupling via the Os-O-B-O-Os 180° route. In addition, the computed magnetic moment on Os ions is $\sim 2 \mu_B$, smaller than the ideal spin-only value. The origin of reduction of the moment at the Os site is twofold. Strong covalency between the Os-5*d* and O-2*p* states partially reduces the moment, inducing a finite magnetic moment ($\sim 0.1 \mu_B$) on the surrounding O atoms. In addition, the antiparallel orbital moment ($\sim -0.1 \mu_B$) further lowers the spin moment in the presence of the spin-orbit coupling. The results are in gratifying agreement with the previous theoretical reports [7,22], confirming the experimental observations [10,14].

In addition, with the help of the DFT calculations, two empirical guiding principles related to electronic structures were established to reveal how the electronic structure of the bridged nonmagnetic B cations and the geometric tilting of octahedra caused by small A ions control the strength of the magnetic interactions and the Néel temperatures. The first general rule is that the magnitude of the magnetic couplings roughly exhibits linear scaling behavior with respect to the reciprocal of the absolute value of energy separation between the occupied Os- t_{2g} and - d states of nonmagnetic B cations. The second one is that the strength of magnetic coupling is related to the degree of the buckling of octahedral

connections. The larger the structural distortion, the smaller the exchange interactions. Moreover, the comparison of these two series helps to distinguish which is more effective to decide the magnetic interactions. The stronger dependence of magnetic interactions on the energy mismatch versus the tilting of octahedra connectivity suggests that the strength of the magnetic coupling is more sensitive to the energy mismatch. In other words, the energy mismatch between the filled Os- t_{2g} and - d states of nonmagnetic B cations is the effective factor to adjust the magnetic coupling, whereas the buckling of octahedra connections is auxiliary.

With the findings in hand, a precise and comprehensive picture for the discrete experimental results in the A_2BOsO_6 system containing the Os⁵⁺-5*d*³ electronic configuration has been established. The principles explain why the Néel temperature of Ba₂InOsO₆ [14] is slightly larger than that of Sr₂InOsO₆ [10], while it is considerably smaller than that of Ca₂ScOsO₆ [11]. Similar arguments can be applied to La₂NaOsO₆ [15] and La₂LiOsO₆ [40]. They are, therefore, expected to be promising candidates worth being investigated for validating our findings. Furthermore, the application of our findings is not limited to the osmates listed above, but can also extend to the analogous iridates and ruthenates, such as Ba₂CaIrO₆ [41] and Ba₂YRuO₆ [42]. For instance, the tendency of variation of Néel temperatures for Sr₂B₂IrO₆ ($B = \text{Mg, Ca, and Zn}$) [43–45] can be explained along with our rules. Hence, these two principles are general and universal for relevant double perovskite $A_2BB'O_6$ oxides, where B is nonmagnetic ions while B' is the magnetic ones including 5*d*³ electronic configurations.

In conclusion, we performed comparative investigations of the electronic and magnetic properties for two series of ordered double perovskite A_2BOsO_6 with nonmagnetic B cations. One is Ba₂BOsO₆ ($B = \text{Sc, Y, and In}$), the other one is A₂ScOsO₆ ($A = \text{Ba, Sr, and Ca}$). According to the results, two empirical guiding principles were achieved to reveal how the electronic configurations of the bridged nonmagnetic B ions and the geometric tilting of octahedra caused by small A ions dictate the strength of the magnetic interactions and the Néel temperatures. One is that the magnitude of the magnetic couplings roughly exhibits linear scaling behavior with respect to the reciprocal of the absolute value of energy separation between the occupied Os- t_{2g} and - d states of nonmagnetic B cations. The other one is that the buckling of octahedral connections decreases the hybridization between Os- t_{2g} and O-2*p* orbitals and the magnitude of overall magnetic exchange couplings, and abates the Néel temperatures as well. Our results not only contribute to a better understanding of the intrinsic magnetic properties of the $A_2BB'O_6$ system containing only magnetic ions B' with 5*d*³ electronic configuration, but also highlight the effective roles of the electronic structure of nonmagnetic B ions and the structural distortion triggered by small A ions in tuning the magnitude of magnetic coupling.

ACKNOWLEDGMENTS

This work was supported by the National Natural Science Foundation of China (Grants No. 21303156 and No. 21543006), the Natural Science Foundation of Hebei

Province (Grants No. B2015203105, No. B2016203158, and No. B2017203113), the Postdoctoral Science Foundation of China (Grant No. 2015M571277), and the Scien-

tific Research Foundation for Returned Scholars. We greatly appreciate the reviewers' constructive comments and insightful suggestions for further improving the manuscript's quality.

- [1] H. L. Feng, M. Arai, Y. Matsushita, Y. Tsujimoto, Y. Gao, C. L. Sathish, X. Wang, Y. Yuan, M. Tanaka, and K. Yamaura, *J. Am. Chem. Soc.* **136**, 3326 (2014).
- [2] Y. Krockenberger, K. Mogare, M. Reehuis, M. Tovar, M. Jansen, G. Vaitheeswaran, V. Kanchana, F. Bultmark, A. Delin, F. Wilhelm, A. Rogalev, A. Winkler, and L. Alff, *Phys. Rev. B* **75**, 020404(R) (2007).
- [3] K.-L. Kobayashi, T. Kimura, H. Sawada, K. Terakura, and Y. Tokura, *Nature* **395**, 677 (1998).
- [4] H. L. Feng, S. Calder, M. P. Ghimire, Y. H. Yuan, Y. Shirako, Y. Tsujimoto, Y. Matsushita, Z. Hu, C. K. Kuo, L. H. Tjeng, T. W. Pi, Y. L. Soo, J. He, M. Tanaka, Y. Katsuya, M. Richter, and K. Yamaura, *Phys. Rev. B* **94**, 235158 (2016).
- [5] J. B. Goodenough, *Magnetism and the Chemical Bonds* (Wiley, New York, 1963).
- [6] M. Zhu, D. Do, C. R. Dela Cruz, Z. Dun, H. D. Zhou, S. D. Mahanti, and X. Ke, *Phys. Rev. Lett.* **113**, 076406 (2014).
- [7] S. Kanungo, B. Yan, C. Felser, and M. Jansen, *Phys. Rev. B* **93**, 161116(R) (2016).
- [8] Y. Xu, S. Liu, N. Qu, Y. Cui, Q. Gao, R. Chen, J. Wang, F. Gao, and X. Hao, *J. Phys.: Condens. Matter* **29**, 105801 (2017).
- [9] M. Zhu, D. Do, C. R. Dela Cruz, Z. Dun, J. -G. Cheng, H. Goto, Y. Uwatoko, T. Zou, H. D. Zhou, S. D. Mahanti, and X. Ke, *Phys. Rev. B* **92**, 094419 (2015).
- [10] A. K. Paul, A. Sarapalova, P. Adler, M. Reehuis, S. Kanungo, D. Mikhailova, W. Schnelle, Z. Hu, C. Kuo, V. Siruguri, S. Rayaprol, Y. Soo, B. Yan, C. Felser, L. H. Tjeng, and M. Jansen, *Z. Anorg. Allg. Chem.* **641**, 197 (2015).
- [11] D. D. Russell, A. J. Neer, B. C. Melot, and S. Derakhshan, *Inorg. Chem.* **55**, 2240 (2016).
- [12] H. L. Feng, C. I. Sathish, J. Li, X. Wang, and K. Yamaura, *Phys. Procedia* **45**, 117 (2013).
- [13] A. W. Sleight, J. Longo, and R. Ward, *Inorg. Chem.* **1**, 245 (1962).
- [14] H. L. Feng, K. Yamaura, L. H. Tjeng, and M. Jansen, *J. Solid State Chem.* **243**, 119 (2016).
- [15] W. R. Gemmill, M. D. Smith, R. Prozorov, and H.-C. zur Loye, *Inorg. Chem.* **44**, 2639 (2005).
- [16] A. A. Aczel, D. E. Bugaris, L. Li, J.-Q. Yan, C. de la Cruz, H.-C. zur Loye, and S. E. Nagler, *Phys. Rev. B* **87**, 014435 (2013).
- [17] Y. Yuan, H. L. Feng, M. P. Ghimire, Y. Matsushita, Y. Tsujimoto, J. He, M. Tanaka, Y. Katsuya, and K. Yamaura, *Inorg. Chem.* **54**, 3422 (2015).
- [18] K. E. Stitzer, M. D. Smith, and H.-C. zur Loye, *Solid State Sci.* **4**, 311 (2005).
- [19] A. S. Erickson, S. Misra, G. J. Miller, R. R. Gupta, Z. Schlesinger, W. A. Harrison, J. M. Kim, and I. R. Fisher, *Phys. Rev. Lett.* **99**, 016404 (2007).
- [20] E. Kermarrec, C. A. Marjerrison, C. M. Thompson, D. D. Maharaj, K. Levin, S. Kroeker, G. E. Granroth, R. Flacau, Z. Yamani, J. E. Greedan, and B. D. Gaulin, *Phys. Rev. B* **91**, 075133 (2015).
- [21] A. E. Taylor, R. Morrow, D. J. Singh, S. Calder, M. D. Lumsden, P. M. Woodward, and A. D. Christianson, *Phys. Rev. B* **91**, 100406(R) (2015).
- [22] A. E. Taylor, R. Morrow, R. S. Fishman, S. Calder, A. I. Kolesnikov, M. D. Lumsden, P. M. Woodward, and A. D. Christianson, *Phys. Rev. B* **93**, 220408(R) (2016).
- [23] S. Bhowal and I. Dasgupta, *Phys. Rev. B* **97**, 024406 (2018).
- [24] G. Kresse and J. Hafner, *Phys. Rev. B* **47**, 558 (1993).
- [25] G. Kresse and J. Furthmuller, *Comput. Mater. Sci.* **6**, 15 (1996).
- [26] J. P. Perdew, K. Burke, and M. Ernzerhof, *Phys. Rev. Lett.* **77**, 3865 (1996).
- [27] V. I. Anisimov, F. Aryasetiawan, and A. I. Lichtenstein, *J. Phys.: Condens. Matter* **9**, 767 (1997).
- [28] V. I. Anisimov, J. Zaanen, and O. K. Andersen, *Phys. Rev. B* **44**, 943 (1991).
- [29] H. Wang, S. Zhu, X. Ou, and H. Wu, *Phys. Rev. B* **90**, 054406 (2014).
- [30] J. P. Perdew, K. Burke, and Y. Wang, *Phys. Rev. B* **54**, 16533 (1996).
- [31] C. Elsässer, M. Fähnle, C. T. Chan, and K. M. Ho, *Phys. Rev. B* **49**, 13975 (1994).
- [32] D. Hobbs, G. Kresse, and J. Hafner, *Phys. Rev. B* **62**, 11556 (2000).
- [33] O. Grotheer, C. Ederer, and M. Fähnle, *Phys. Rev. B* **63**, 100401 (2001).
- [34] C. S. Helberg, W. E. Pickett, L. I. Boyer, H. T. Stokes, and M. J. Mehl, *J. Phys. Soc. Jpn.* **68**, 3489 (1999).
- [35] N. Lampis, C. Franchini, G. Satta, A. Geddo-Lehmann, and S. Massidda, *Phys. Rev. B* **69**, 064412 (2004).
- [36] P. W. Anderson, *Phys. Rev.* **115**, 2 (1959).
- [37] M. Liu, C.-E. Hu, and X.-R. Chen, *Inorg. Chem.* **57**, 4441 (2018).
- [38] S. Gangopadhyay and W. E. Pickett, *Phys. Rev. B* **93**, 155126 (2016).
- [39] C. Franchini, T. Archer, J. He, X.-Q. Chen, A. Filippetti, and S. Sanvito, *Phys. Rev. B* **83**, 220402(R) (2011).
- [40] D. D. Maharaj, G. Sala, C. A. Marjerrison, M. B. Stone, J. E. Greedan, and B. D. Gaulin, *Phys. Rev. B* **98**, 104434 (2018).
- [41] J. Park, J. G. Park, I. P. Swainson, H.-C. Ri, Y. N. Choi, C. Lee, and D.-Y. Jung, *J. Korean Phys. Soc.* **41**, 118 (2002).
- [42] T. Aharen, J. E. Greedan, F. Ning, T. Imai, V. Michaelis, S. Kroeker, H. D. Zhou, C. R. Wiebe, and L. M. D. Cranswick, *Phys. Rev. B* **80**, 134423 (2009).
- [43] P. Kayser, M. J. Martinez-Lope, J. A. Alonso, M. Retuerto, M. Croft, A. Ignatov, and M. T. Fernandez-Diaz, *Inorg. Chem.* **52**, 11013 (2013).
- [44] D. Y. Jung and G. Demazeau, *J. Solid State Chem.* **115**, 447 (1995).
- [45] P. Kayser, M. J. Martinez-Lope, J. A. Alonso, M. Retuerto, M. Croft, A. Ignatov, and M. T. Fernandez-Diaz, *Eur. J. Inorg. Chem.* **2014**, 178 (2014).